Analysis of the F-actin binding fragments of vinculin using stopped-flow and dynamic light-scattering measurements

Wolfgang H. GOLDMANN[1], Zeno GUTTENBERG[1], Jay X. TANG[2], Klaus KROY[3], Gerhard ISENBERG[3] and Robert M. EZZELL[1]

[1] Department of Surgery, Surgery Research Laboratories, Massachusetts General Hospital, Harvard Medical School, Charlestown MA, USA
[2] Division of Experimental Medicine, Brigham and Women's Hospital, Harvard Medical School, Boston MA, USA
[3] Physik Department der Technischen Universität München, Garching, Germany

Using amino acids 884−1066 and 884−1012 expressed from chicken vinculin as fusion proteins with schistosomal glutathione *S*-transferase, we determined the binding kinetics of the protein fragments with F-actin. We established by the stopped-flow method a two-step binding process: an initial rapid reaction followed by a slower process. The latter is attributed to F-actin cross-linking and/or bundling, which was previously detected by viscometry and electron microscopy [Johnson, R. P. & Craig, S. W. (1995) *Nature 373*, 261−264]. This is also supported by dynamic light-scattering measurements, indicating dramatic changes in the internal actin filament dynamics, i.e. in bending undulations due to thermal noise. The similar size of the binding reaction for both fusion proteins with F-actin indicates that the F-actin binding site(s) on vinculin are located between residues 884−1012. No binding of pure glutathione *S*-transferase or its fusion protein with vinculin peptide 1012−1066 with F-actin was detected by either method.

Keywords: vinculin; actin; stopped-flow kinetics; dynamic light scattering.

Vinculin is a cytoskeletal protein (117 kDa, 1066 amino acids) that is concentrated in focal adhesion plaques and thought to play a major structural role in attaching integrins to the actin cytoskeleton. In cell−cell adherent junctions, vinculin is closely associated with the cadherin/catenin complex. In its active form, vinculin interacts with a number of focal contact proteins through several domains that have been mapped (cf. [1]). At the NH$_2$-terminus, vinculin binds to talin (residues 1−258) [2−4] and at a shorter region within this fragment to α-actinin (residues 1−107) [5, 6]. The COOH-terminal region of vinculin contains binding sites for paxillin (residues 978−1000) [7, 8], acidic phospholipids (residues 935−978, 1020−1040) [9], and actin (residues 884−1066) [10−13]. The intervening central sequences in vinculin have unknown functions but include a tyrosine phosphorylation site (residue 822) and three repeating proline-rich regions (residues 837−847, 860−878) [14], one of which binds to a vasodilator-stimulated phosphoprotein [15, 16].

Recent studies by Johnson and Craig [12] have convincingly demonstrated that the globular head domain (residues 1−851) and extended tail domain (residues 858−1066) of vinculin can fold to mask a principal functional domain. A high-affinity intramolecular interaction between the NH$_2$-head and COOH-tail is believed to be responsible for preventing acidic phospholipids and F-actin from binding to vinculin. One important issue is, therefore, to define the F-actin binding regions on vinculin and to ascertain the binding affinities. In the present study we used stopped-flow and dynamic light-scattering methods to determine the binding reactions of F-actin with two fragments of the vinculin molecule.

MATERIALS AND METHODS

Protein preparation. Actin was prepared according to the procedure of Spudich and Watt [17] from acetone powder obtained from rabbit back muscle. The protein concentration was determined using $\varepsilon_{290} = 26460 \ M^{-1} \ cm^{-1}$. G-actin was stored in buffer G (2 mM Tris/HCl pH 7.5, 0.2 mM CaCl$_2$, 0.5 mM ATP, 0.2 mM dithiothreitol and 0.005% NaN$_3$), either kept on ice for less than two days or rapidly frozen using liquid nitrogen, kept at −80°C, and thawed right before use. For the light-scattering studies, G-actin was polymerized overnight at 4°C in buffer F (2 mM Tris/HCl pH 7.5, 100 mM KCl, 2 mM MgCl$_2$, 0.2 mM CaCl$_2$, 0.2 mM dithiothreitol and 0.5 mM ATP).

Amino acids 884−1066, 884−1012, and 1012−1066 of chicken vinculin expressed as fusion proteins with schistosomal glutathione *S*-transferase (GST) were generous gifts from Drs Susan Craig and Robert Johnson (Johns Hopkins University, Baltimore). The fusion proteins, referred to as GST/V884−1066, GST/V884−1066 and GST/V1012−1066, were purified according to [18], except that the expressed proteins were eluted from the glutathione−agarose affinity resin with 50 mM Tris/HCl pH 8.5 and 25 mM reduced glutathione. Protein concentrations were determined with the Bio-Rad protein assay reagent, using GST as standard. GST concentration was determined as $A_{280}^{1\%} = 20$ [11].

The purity of the fusion proteins was examined by SDS/PAGE shown in Fig. 1. Prior to experimentation, the fusion proteins were dialyzed for 2 h at 4°C in buffer (10 mM Tris/HCl pH 7.5, 150 mM NaCl, 1 mM EGTA, 0.3 mM NaN$_3$, and 0.1 mM EDTA).

Correspondence to W. H. Goldmann, Massachusetts General Hospital, Harvard Medical School, Department of Medicine, Building 149, 13th Street, Charlestown, MA 02129, USA
Fax: +1 617 726 5669.
E-mail: goldman@helix.mgh.harvard.edu
URL: http://www.mgh.harvard.edu/
Abbreviations. GST, glutathione *S*-transferase; GST/V884−1066, GST/V884−1066 and GST/V1012−1066, fusion proteins of GST and chicken vinculin peptides 884−1066, 884−1066 and 1012−1066.
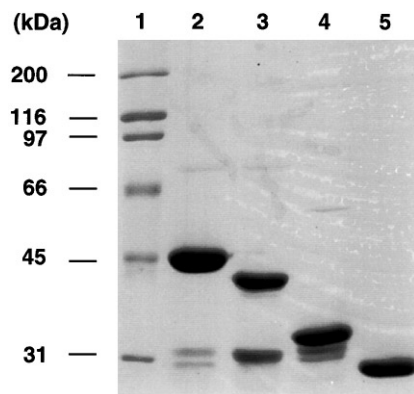*Note.* The first three authors contributed equally to this work.

Fig. 1. SDS gel electrophoresis. 5−10% gradient SDS gel showing molecular mass markers (lane 1), GST/V884−1066 (lane 2), GST/V884−1012 (lane 3). GST/V1012−1066 (lane 4), and GST (lane 5). Lanes (2−5) were each loaded with approximately 3 μg protein.

Stopped-flow method. All experiments were performed in a hybrid ultraviolet/visible stopped-flow spectrophotometer (SF-61; Hi-Tech Scientific Ltd, as shown in [19]). Briefly, F-actin (6 μM) and fusion proteins (at various concentrations) were held separately in two driving syringes, and a drive plate was used to drive the syringes at a burst pressure of 400 kPa, causing them to mix rapidly, initiating a new reaction while displacing the solution from the previous run as the reaction mixture was driven into the observation cell. The flow was stopped by a plunger after a flow of 100 μl fluid volume. The travel of the stop plunger was set by a rigid stopping block causing rapid deceleration of the solutions and triggering the data acquisition system. The dead time of the apparatus was ≈2 ms. The optical system consisted of a 100-W mercury lamp (Osram HBO 100W/2) with the monochromator set at 355 nm and a slit spectral width of 2 nm. The light was transmitted via a light guide to the mixing/observation chamber and the emitted light monitored at 90° by the photomultiplier. The signal captured by the photomultiplier was electronically filtered by a unity gain amplifier. The time constant was normally set at 0.1% of the total sweep time. Voltage output from the photomultiplier was digitized by an analog converter before being transferred to a Macintosh computer IIfx and analyzed by a commercially available program (IGOR Pro 3). A 5−10% pretrigger was normally used for data collection. Temperature was regulated by an external water bath with less than 0.1 °C variation.

Theoretical basis of binding kinetics (stopped-flow). For a chemical reaction of two reactants A and B resulting in a product C (A+B⇔C), the time-dependent concentration of the product ([C]) satisfies the following differential equation:

$$\frac{d[C]}{dt} = k_{+1}([A][B]) - k_{-1}[C] \qquad (1)$$

where t is time; [A] and [B] are concentrations of A and B at time t; k_{+1} and k_{-1}, are the on and off rate constants, respectively.

The general solution to Eqn (1) can be expressed as follows (cf. [20])

$$[C] = [C]^F \left\{ 1 - \frac{e^{-kt}}{1 + (k_{+1}/k)[C]^F(1 - e^{-kt})} \right\}, \qquad (2)$$

where

$$k = k_{+1}([A]^F + [B]^F) + k_{-1}. \qquad (3)$$

The superscript F indicates final concentrations, which can be determined from Eqn (1) at $t = \infty$ when the reaction reaches

equilibrium, hence $d[C]/dt = 0$. Note that Eqn (2) is a modified version of Eqn (4.80) in [20], except that for the stopped-flow study the initial concentration of the product is zero, i.e. $[C]^0 = 0$ at $t = 0$.

In a simple extreme, when the initial reactant concentration [A] is in excess over [B], [C] can be derived as follows:

$$[C] = [C]^F (1 - e^{-kt}) \qquad (4)$$

where

$$k = k_{+1}[A]^0 + k_{-1} \qquad (5)$$

with $[A]^0$ the concentration of A at $t = 0$. We assume that the change of the scattered light intensity, I during the reaction is proportional to the concentration of product, [C]. Therefore, the reaction constant k can be calculated using an exponential fit to the measured data points from stopped-flow experiments. Using different concentrations of an excess reactant, the association and dissociation rate constants can be obtained from a k versus $[A]^0$ plot. Note that, in the following measurements, the photomultiplier was adjusted to gain optimal sensitivity and no attempt was made to determine the final concentration $[C]^F$ based on the electronic output (V) which is linear with the final scattering intensity only at fixed settings.

Dynamic light-scattering setup. A light-scattering apparatus supplied by Brookhaven Instruments, model BI-2030, was used throughout as shown in [21]. A spectral line (633 nm) from a 10-mW He-Ne laser was used as light source, which was transmitted through the sample held in a glass tube of 8 mm inner diameter. A large quartz beaker in the goniometer was filled with decalin to reduce reflection at the surface of the glass tube. The cell was temperature-controlled and the swivel arm could be regulated continuously between 10−170°C. The aperture in the light path prior to the photomultiplier was set to minimize stray light. Light detected from the photomultiplier was directly transmitted to the correlator and analyzed by a computer. The slit width for receiving the scattered light is set at 800 nm. Other experimental parameters are preset and computer-controlled.

Analysis of dynamic light-scattering data. The dynamic structure factor $g(q,t)$, which gives information about the internal dynamics of polymers, can be calculated from the intensity autocorrelation function $g^{(2)}(q,t)$ of scattered light, via a simple relationship $g^{(2)}(q,t) = g(q,t)^2$. Since the temporal decrease of this function is due to the thermal undulations of polymers, which lead to a decay of their spatial self-correlation, its characteristic decay time gives information on the local mobility. Actin solutions in the presence of cross-linking/bundling proteins, in particular, have been described by Goetter et al. [22] to cause a dramatic immobilization of actin filaments which results in a much slower decay of the correlations. These authors gave a theoretical description of the dynamic structure factor $g(q,t)$ of F-actin solutions using the function $g(q,t) \propto \exp(-bt^{3/4})$, where q is the scattering vector, t is the correlation time, and b is a function of temperature, scattering vector, actin concentration, filament length and stiffness. More specifically, for dilute and semidilute F-actin solutions, b can be expressed by the decay rate γ_q via $b \propto \gamma_q^{3/4}$ with $\gamma_q = (k_B T/\zeta_\perp)q^{8/3}L_p^{-1/3}$ where $\zeta_\perp$ is the friction coefficient/length of the polymer and L_p is the persistence length. In particular, b has a quadratic dependence on the scattering vector q. For further details of the calculation of the dynamic structure factor, we refer the reader to [22, 23]. The authors of these papers pointed out that the above expression for $g(q,t)$ gives an excellent fit to the measured structure factor of F-actin in the range of $10^{-5}−10^{-2}$ s. They also observed that for actin filaments, stiffened by adding tropomyosin/troponin, the measured curves of $g(q,t)$ are time-shifted images of the refer-
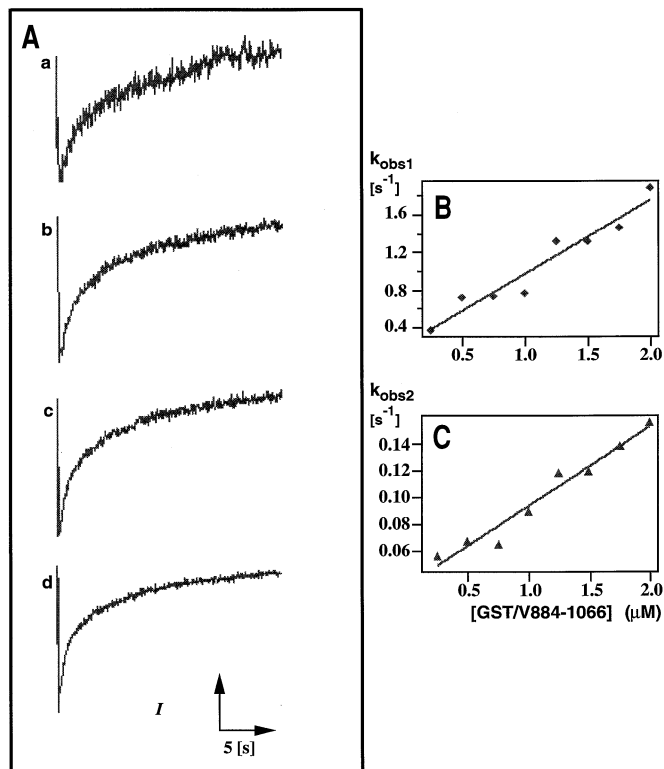
Fig. 2. Stopped-flow analysis. The traces in (A) each represent an average of five consecutive measurements in the stopped-flow apparatus. Changes in light-scattering intensity, I (at 90° angle and 355 nm wavelength) were detected at (a) 0.5 µM, (b) 1 µM, (c) 1.5 µM, and (d) 2 µM fusion protein (GST/V884−1066) with 3 µM F-actin (concentrations after mixing in the reaction cell). Conditions: temperature, 25°C; buffer, 0.2 mM Tris/HCl pH 7.5, 100 mM KCl, 2 mM MgCl$_2$, 1 mM EGTA, 2 mM CaCl$_2$, 0.2 mM dithiothreitol and 0.5 mM ATP. (B) Plot of the first observed rate, k_{obs1} and (C) second observed rate k_{obs2} against various fusion protein concentrations. The best-fit lines to the data give a value of $k_{-1} = 0.38$ s^{-1} (B) and $k_{-2} = 0.035$ s^{-1} (C) for the intercept and a slope of $k_{+1} = 6.5 \times 10^5$ M$^{-1} \times$s^{-1} (B) and $k_{+2} = 5.2 \times 10^4$ M$^{-1} \times$s^{-1} (C).

Fig. 3. Stopped-flow analysis. The traces in (A) each represent an average of five consecutive measurements in the stopped-flow apparatus. Changes in light-scattering intensity, I (at a 90° angle and 355 nm wavelength) were detected at (a) 0.5 µM, (b) 1 µM, (c) 1.5 µM, and (d) 2 µM fusion protein (GST/V884−1012) with 3 µM F-actin (concentrations after mixing in the reaction cell). (B) Plot of the first observed rate, k_{obs1} and (C) second observed rate k_{obs2} against various fusion protein concentrations. The best-fit lines to the data give a value of $k_{-1} = 0.7$ s^{-1} (B) and $k_{-2} = 0.065$ s^{-1} (C) for the intercept and a slope of $k_{+1} = 5.6 \times 10^5$ M$^{-1} \times$s^{-1} (B) and $k_{+2} = 3.8 \times 10^4$ M$^{-1} \times$s^{-1} (C). Conditions are the same as in Fig. 2.

Table 1. Association and dissociation rate constants for vinculin fusion proteins GST/V884–1066 and GST/V884–1012 in their binding of F-actin. Conditions are described in legends to Figs 2 and 3.

Fusion protein	k_{+1}	k_{-1}	k_{+2}	k_{-2}
	M$^{-1} \times$s^{-1}	s^{-1}	M$^{-1} \times$s^{-1}	s^{-1}
GST/V884−1066	0.65×10^6	0.38	0.054×10^6	0.035
GST/V884−1012	0.56×10^6	0.70	0.038×10^6	0.065

ence curve, as predicted for stiffer polymers from the functional dependence of b on L_p given above.

We previously reported results for F-actin solutions in the presence of talin, where we observed quite a similar time shift in the structure factor at low talin concentrations (see Fig. 5 [21]). For higher talin concentrations, the structure factor showed increasing deviations from the stretched exponential form, and the decay of the structure factor was slowed down considerably. Similar findings in this study with the vinculin fragments GST/V884−1066 and GST/V884−1012 are interpreted as follows: from our kinetic data, we assume that these proteins lead to bundling and/or cross-linking of actin filaments. Individual bundles should still behave similarly to stiffened actin filaments which explains the time-shifted curves for $g(q,t)$ in the case of weak cross-linking. At higher concentrations of the cross-linking proteins, the network becomes an increasingly rigid and immobile network of cross-linked filaments and bundles which may no longer be described as a solution of freely undulating semiflexible polymers. Hence, the decay of temporal correlations slows down significantly, accompanied by the deviations from the stretched exponential form for high vinculin concentrations. What is measured at the longer time scale are the collective viscoelastic modes of this rigidly cross-linked structure, and the characteristic decay time of $g(q,t)$ is an indica-
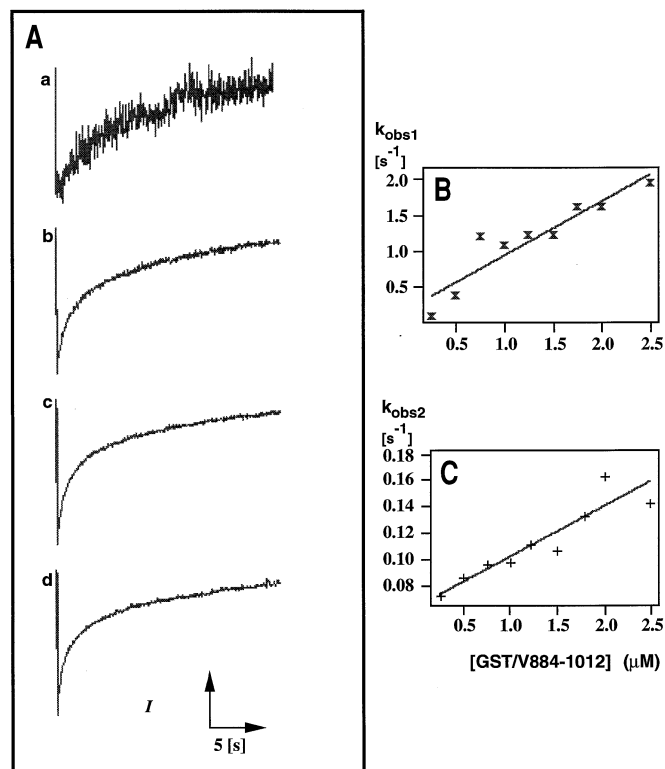
tion of the rigidity of its dominant modes on length scales of about $1/q$.

To extend the quantitative analysis of [22] to cross-linked networks, a theory for the dynamics of such inhomogenously cross-linked semiflexible polymer networks would be needed, which is not yet available. Instead, in this experimental study, we tabulate the parameter b as a semi-quantitative measure of the decreasing mobility of the polymers with increasing vinculin concentration.

RESULTS

Stopped-flow studies. The association reaction between F-actin and the fusion proteins GST/V884−1066 and GST/V884−1012 were studied, using the change in light-scattering intensity, I, at
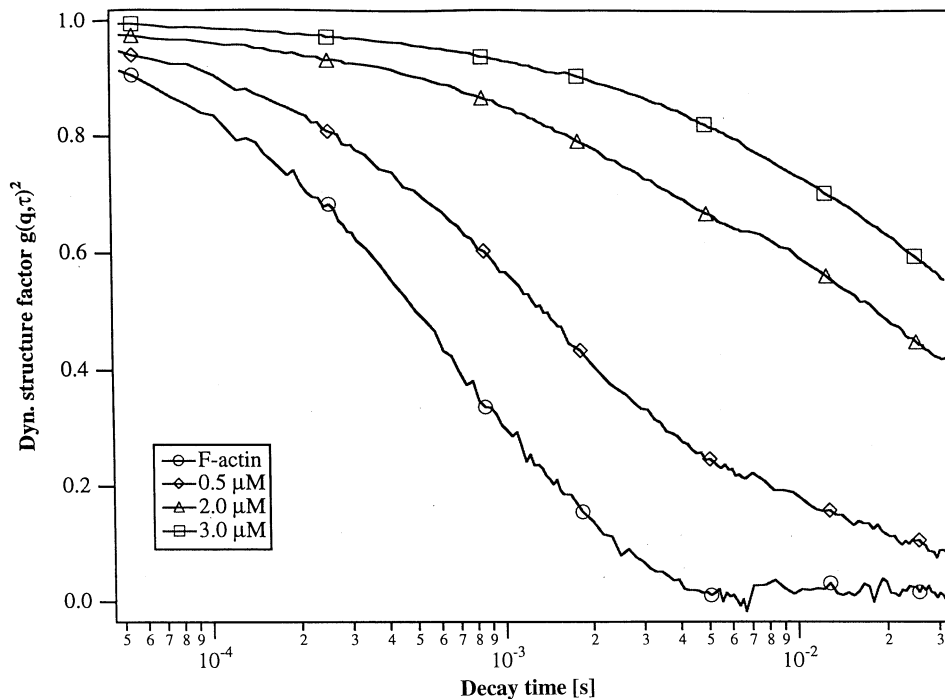
Fig. 4. Dynamic light-scattering experiments. The squared dynamic structure factor is plotted against the correlation time (between $0.05-30$ ms) of 3 μM F-actin solutions in the absence and presence of 0.5, 2, and 3 μM (GST)/V884$-$1066 fusion proteins, respectively. Conditions: temperature, 22 °C; measuring time, 10 min; wavelength, 633 nm; solvent conditions are the same as in Fig. 2. (Note: g is the dynamic structure factor, q is the scattering vector, and t is the correlation time, b is a function of temperature, scattering vector, actin concentration, filament length and stiffness as explained in the text.)

355 nm. Each curve in Figs 2A and 3A is an average of five measurements of transient kinetics. A fit to the curves according to Eqn (2) showed deviations from the data points and a sum of such terms to incorporate independent binding pathways would contain too many fit parameters to obtain meaningful results. However, a sum of two terms according to Eqn (4) results in a much simplified two-exponential fit. This practical approach can be partially justified by the knowledge that each fusion protein used in this study binds F-actin with relatively low stoichiometry of 1:2$-$4 [12], and hence the condition of excess reactant, i.e. the fusion proteins, roughly holds even though they were only comparable in molarity with actin in our measurements. Indeed, we found experimentally that the decay in intensity could be adequately described by two exponentials at various concentrations. Assuming that the equations

$$k_{obs1} = k_{+1} \cdot [A]^0 + k_{-1}$$

and

$$k_{obs2} = k_{+2} \cdot [A]^0 + k_{-2}$$

describe two separate reactions under the much simplified condition, the observed rates k_{obs1} and k_{obs2} with respect to $[A]^0$ determine the values of k_{+1} and k_{+2} of the two reactions, where $[A]^0$ is the concentration of GST/V884$-$1066 or GST/V884$-$1012, respectively. Plotting the observed rates against the various fusion protein concentrations, we obtained the association rate constants from the slopes and the dissociation rate constants from the intercepts. The binding constants for F-actin and the fusion proteins were obtained through the fits shown in Figs 2B, 3B, 2C and 3C; the results are summarized in Table 1.

In control experiments, mixing F-actin and GST under the same conditions resulted in no intensity change, i.e. no binding event occurred. Furthermore, when F-actin, was mixed with various concentrations (up to 6 μM) of GST/V1012$-$1066, again no detectable intensity change was observed during the transient

kinetic measurements. These results suggest that neither pure GST nor the fusion protein GST/V1012$-$1066 is involved in the binding events (data not shown).

Dynamic light-scattering studies. Prior to measuring the effects of vinculin fragments on the light-scattering behavior of the F-actin network, we tested the expression for $g(q,t)$ by measuring pure F-actin solutions. Normalizing the amplitude of the autocorrelation function at $t = 0$, the data were fitted accurately over the entire time range, and the dependency of the scattering angle followed the q^2 law. To study the scattering behavior of F-actin solutions in the presence of fusion proteins, we incubated GST/V884$-$1066 and GST/V884$-$1012 at various concentrations. Results from these experiments are shown in Figs 4 and 5, where we plot the function $g(q,t)^2$, for a more convenient presentation, against decay time at a fixed scattering angle of 90°. The increase in fusion protein concentration corresponds to a gradual change in curve structure. Fitting the function to the data, we determined the constant b. Examples of the fit function $g(q,t) \propto \exp(-bt^{3/4})$ are shown in Fig. 6 as solid curves, superimposed on the light-scattering curves (taken from Fig. 5) of pure F-actin solutions and F-actin in the presence of 0.25$-$2.0 mM GST/V884$-$1012. Figs 4$-$6 and Table 2 for the parameter b show with increasing fusion protein concentration a progressive decrease of the decay, which is most likely due to strong cross-linking and bundle formation in the F-actin solution, as confirmed by other studies [11, 12]. We emphasize that the fits cannot be expected to allow for a rigorous quantitative analysis in terms of model parameters of the single actin filaments such as L_p and $\zeta_\perp$ in the presence of vinculin. Instead, we present in Table 2 a semi-quantitative measure of the decreasing mobility of the polymers with increasing vinculin concentration. Despite the lack of a rigorous quantitative interpretation, the results given in Table 2 strongly indicate that both GST/V884$-$
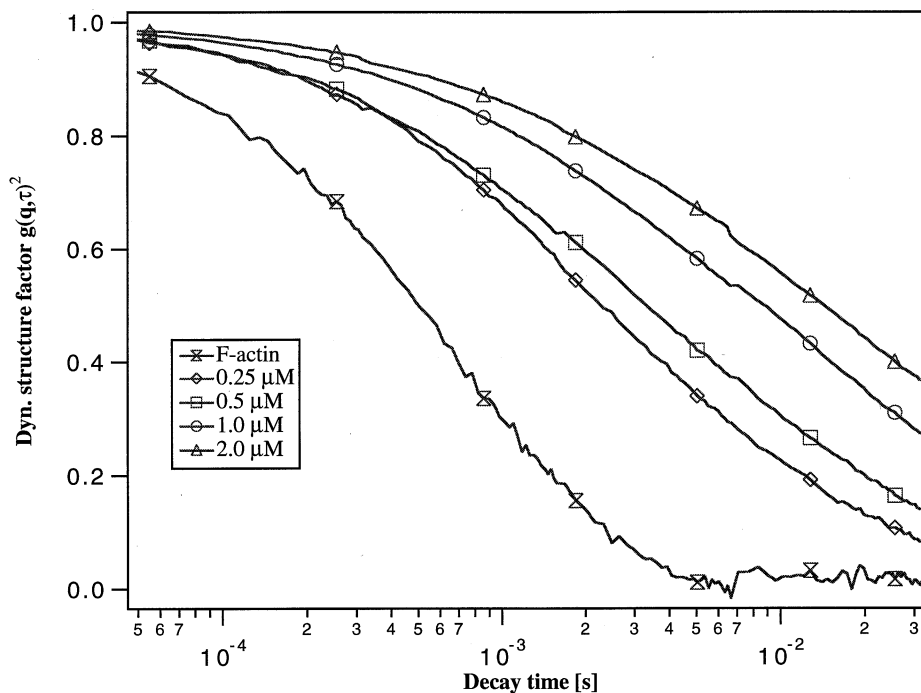
Fig. 5. Dynamic light-scattering experiments. The squared dynamic structure factor is plotted against the correlation time (between of 0.05−30 ms) of 3 μM F-actin solutions in the absence and presence of 0.25, 0.5, 1, and 2 μM (GST)/V884−1012 fusion proteins. The experimental conditions are the same as in Fig. 4 but with a different fusion protein.
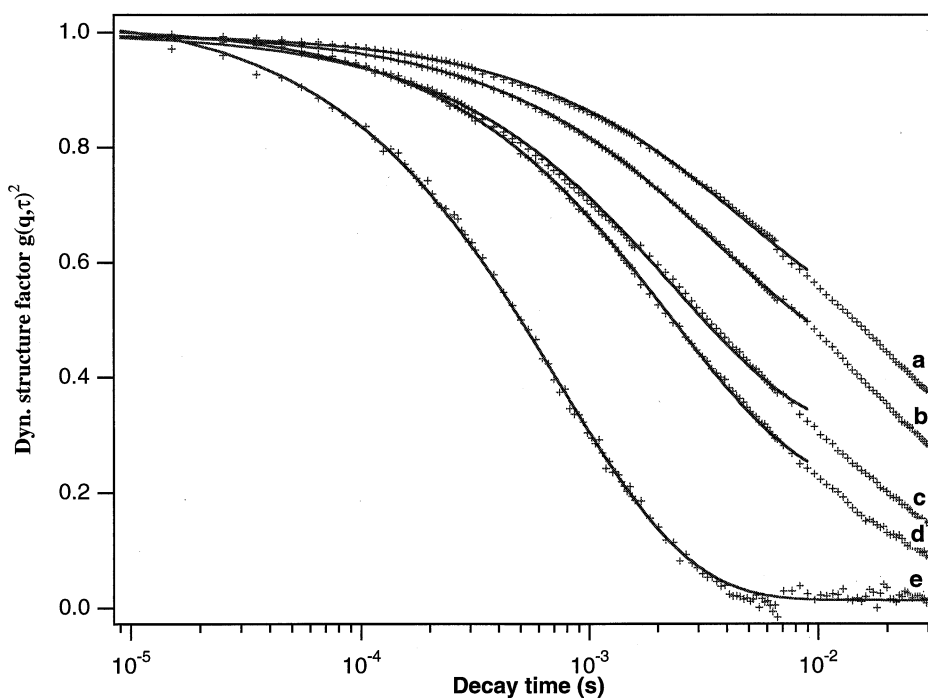

Fig. 6. Dynamic light-scattering analyses. Plots of the squared dynamic structure factor for an F-actin solution in the presence of 0.25 μM (d), 0.5 μM (c), 1.0 μM (b), 2.0 μM (a) GST/V884−1012 and pure F-actin solution (e) obtained in Fig. 5. Superimposed are the calculated profiles of $g(q, t) \propto \exp(-bt^{3/4})$. For pure F-actin solutions the data points coincide with the theory of [22]. The measurements of F-actin in the presence of vinculin fusion proteins show deviations from the theory at long times. This behavior is attributed to strong cross-linking and bundle formation. For decay times $\lesssim 10$ ms, the value for the prefactor b can be determined from the data points. For the calculation of the dynamic structure factor for solutions of semiflexible polymers see [22, 23].

1066 and GST/V884−1012 have significant influence on the internal dynamics of actin filaments. In contrast, no change in autocorrelation profile occurred to F-actin in the presence of pure GST and the fusion protein GST/V1012−1066 up to 6 μM (data not shown).

DISCUSSION

In the present study we used stopped-flow measurements to determine the binding parameters of vinculin fusion proteins with F-actin and confirmed their binding by dynamic light scat-

Table 2. The influence of increasing vinculin fusion protein concentration of GST/V884–1066 and GST/V884–1012 with F-actin on *b* compared with pure F-actin. The experimental conditions are described in the legend to Fig. 4 as well as the meaning of the parameter *b*. Zero concentration of fusion protein indicates pure F-actin.

Fusion protein	Concn	$g(q,t) \propto \exp(-bt^{3/4})$
	μM	
GST/V884−1066	0	108.7
	0.5	60.1
	2.0	43.2
	3.0	25.4
GST/V884−1012	0	108.7
	0.25	63.1
	0.5	55.0
	1.0	33.3
	2.0	24.4

tering. Previously, Johnson and Craig [11, 12] have shown, using cosedimentation assays, that the amino acid stretch 811−1066 of vinculin is the potential binding region for F-actin. These researchers observed a specific interaction of actin with the C-terminal region on vinculin and determined the equilibrium dissociation constant K_d for the fusion protein GST/V811−1066 and the 30-kDa fragment (V811−1066) to be 0.6−0.8 μM and ≈2 μM, respectively.

We were interested in studying the binding event by using transient kinetics methods. For this reason we employed the stopped-flow apparatus which allowed the determination of association and dissociation rate constants of these species. Measuring the association of F-actin with fusion protein complexes (GST/V884−1066 and GST/V884−1012), we noticed two binding reactions that differed in the rate constant by a factor of ≈10. The distinct relaxations could be described as a fast binding event followed by a slower process. Johnson and Craig [12] observed in falling ball viscometric and electron microscopic studies that F-actin solutions in the presence of fusion protein GST/V811−1066, as well as vinculin 30-kDa fragments, form gels in a concentration-dependent manner. The kinetic events described here can, therefore, be attributed to two successive processes, an initial binding followed by cross-linking and/or bundling events. Further support for this notion comes from the dynamic light-scattering data, where we observed increasing stiffness of the F-actin network concomitant with increasing fusion protein concentration. The equilibrium dissociation constant K_d calculated from the ratio of k_{-1}/k_{+1} for the overall binding reactions (K_d between 0.5−1.5 μM), also agrees well with the published data [11, 12]. In contrast, using intact vinculin or the 90-kDa head fragment of vinculin with actin, Johnson and Craig [12] did not observe these events. In previous studies using rheology and dynamic light scattering, we also showed that intact vinculin produces only negligible changes in filament stiffness when mixed with F-actin [24, 25].

Since both GST/V884−1066 and GST/V884−1012 are shown to not only bind but also cross-link F-actin, one interesting question remains as to whether the C-terminal fragments of vinculin contain at least two actin binding sites. It is unlikely that the cross-linking activity of these two fusion proteins are due to the dimerization of GST since the 30-kDa fragment V811−1066 also cross-links F-actin [12]. However, it has been recently proposed that lateral aggregation of F-actin does not necessarily require dual binding sites on the actin bundling protein [26−28], and shielding of surface charge of F-actin due to the binding of either polyvalent cations or cationic protein li-

gands suffices to induce actin bundle formation, or cross-linking of actin filaments. Therefore, the measured cross-linking or bundling activity of the GST-vinculin fragments does not necessarily suggest that there are two or more actin binding sites involved on each fusion protein. Nevertheless, such drastic changes occurred to the actin filaments arrangement *in vitro* help demonstrate the potential function of the actin binding domain of vinculin when it is activated by breaking the intramolecular association.

The conflicting evidence over the years concerning whether intact vinculin binds to actin has probably been resolved by accepting the model that the binding site of actin (and probably of α-actinin, talin, and acidic phospholipids) on vinculin can be masked by a high-affinity head−tail intramolecular interaction ($K_d \approx 50$ nM) of vinculin [11, 12]. We and others have demonstrated that actin binds to vinculin at an affinity of $K_d \approx 1$ μM in appropriate conditions [29−32]. The mechanism of intramolecular association may be controlled by either intracellular or extracellular signaling events, i.e. regulation by members of the Rho family, phosphorylation [33, 34], or binding of acidic phospholipids [35]. Elucidation of such a mechanism will be essential for understanding the formation of focal adhesion complexes. Proteins that are absolutely required for the formation and function of focal adhesions continue to be the subject of ongoing research, as described in recent reviews [1, 36−40].

REFERENCES

1. Jockusch, B. M., Bubeck, P., Giehl, K., Kroemker, M., Moschner, J., Rotkegel, M., Ruediger, M., Schiller, K., Stanke, G. & Winkler, J. (1995) The molecular architecture of focal adhesion, *Annu. Rev. Cell Dev. Biol. 11*, 379−416.
2. Burridge, K. & Mangeat, P. (1984) An interaction between vinculin and talin, *Nature 308*, 744−746.
3. Critchley, D. R., Gilmore, A., Hemmings, L., Jackson, P., McGregor, A., Ohanian, V., Patel, B., Waites, G. & Wood, C. (1991) Cytoskeletal proteins in adherens-type cell-matrix junctions, *Biochem. Soc. Trans. 19*, 1028−1033.
4. Gilmore, A. P., Jackson, P., Waites, G. T. & Critchley, D. R. (1992) Further characterization of the talin-binding site in the cytoskeletal protein vinculin, *J. Cell Sci. 103*, 719−731.
5. Belkin, A. M. & Koteliansky, V. E. (1987) Interaction of iodinated vinculin, metavinculin, and alpha-actinin with cytoskeletal protein, *FEBS Lett. 220*, 291−294.
6. Menkel, A. R., Kroemker, M., Bubeck, P., Ronsiek, M., Nikolai, G. & Jockusch, B. M. (1994) Charaterization of an F-actin-binding domain in the cytoskeletal protein vinculin, *J. Cell Biol. 126*, 1231−1240.
7. Turner, C. E., Glenney, J. R. Jr & Burridge, K. (1990) Paxillin: a new vinculin-binding protein present in focal adhesions, *J. Cell Biol. 111*, 1059−1068.
8. Wood, C. K., Turner, C. E., Jackson, P. & Critchley, D. R. (1994) Characterisation of the paxillin-binding site and the C-terminal focal adhesion targeting sequence in vinculin, *J. Cell Sci. 107*, 709−717.
9. Tempel, M., Goldmann, W. H., Isenberg, G. & Sackmann, E. (1995) Interaction of the 47-kDa talin fragment and the 32-kDa vinculin

fragment with acidic phospholipids: a computer analysis, *Biophys. J. 69*, 228−241.

10. Kroemker, M., Ruediger, A. H., Jockusch, B. M. & Rüdiger, M. (1994) Intramolecular interactions in vinculin control alpha-actinin binding to the vinculin head, *FEBS Lett. 355*, 259−262.

11. Johnson, R. P. & Craig, S. W. (1994) An intramolecular association between the head and tail domains of vinculin modulates talin binding, *J. Biol. Chem. 269*, 12611−12619.

12. Johnson, R. P. & Craig, S. W. 1995 F-actin binding site masked by the intramolecular association of vinculin head and tail domains, *Nature 373*, 261−264.

13. Johnson, R. P. & Craig, S. W. (1995) The carboxy-terminal tail domain of vinculin contains a cryptic binding site for acidic phospholipids, *Biochem. Biophys. Res. Commun. 210*, 159−164.

14. Moiseyeva, E. P., Weller, P. A., Zhidhova, N. I., Corben, E. B., Patel, B., Jasinska, I., Koteliansky, V. E. & Crichtley, D. R. (1993) Organization of the human gene encoding the cytoskeletal protein vinculin and the sequence of the vinculin promoter, *J. Biol. Chem. 268*, 4318−4325.

15. Brindle, N. P. J., Holt, M. R., Davies, J. E., Price, C. J. & Critchley, D. R. (1996) The focal-adhesion vasodilator-stimulated phosphoprotein (VASP) binds to the proline-rich domain in vinculin, *Biochem. J. 318*, 753−757.

16. Reinhard, M., Ruediger, M., Jockusch, B. M. & Walter, U. (1996) VASP interaction with vinculin: a recurring theme of interactions with proline-rich motifs, *FEBS Lett. 399*, 103−107.

17. Spudich, J. A. & Watt, S. (1971) The regulation of rabbit skeletal muscle contraction. I. Biochemical studies of the interaction of the tropomyosin-troponin complex with actin and the proteolytic fragments of myosin, *J. Biol. Chem. 246*, 4866−4871.

18. Smith, D. B. & Johnson, K. S. (1998) Single-step purification of polypeptides expressed in *Escherichia coli* as fusions with glutathione *S*-transferase, *Gene 67*, 31−40.

19. Goldmann, W. H., Guttenberg, Z., Ezzell, R. M. & Isenberg, G. (1998) The study of fast reactions by the stopped flow method, in *Modern optics, electronics, and high precision techniques in cell biology* (Isenberg, G., ed.) pp. 161−172, Springer-Verlag, Heidelberg.

20. Hiromi, K. (1979) *Kinetics of fast enzyme reactions*, John Wiley & Sons, New York.

21. Goldmann, W. H., Guttenberg, Z., Kaufmann, S., Hess, D., Ezzell, R. M. & Isenberg, G. (1997) Examining F-actin interaction with intact talin and talin head and tail fragment using static and dynamic light scattering, *Eur. J. Biochem. 250*, 447−450.

22. Goetter, R., Kroy, K., Frey, E., Baermann, M. & Sackman E. (1995) Dynamic light scattering from semidilute actin solutions: a study of hydrodynamic screening, filament bending stiffness, and the effect of tropomyosin/troponin-binding, *Macromolecules 29*, 30−36.

23. Kroy, K. & Frey, E. (1997) Dynamic scattering from solutions of semiflexible polymers, *Phys. Rev. E 55*, 3092−3101.

24. Ruddies, R., Goldmann, W. H., Isenberg, G. & Sackmann, E. (1993) The viscoelasticity of entangled networks: the influence of defects and the modulation by talin and vinculin, *Eur. Biophys. J. 22* 309−321.

25. Goetter, R., Goldmann, W. H. & Isenberg, G. (1995) Internal actin filament dynamics in the presence of vinculin: a dynamic light scattering study, *FEBS Lett. 359*, 220−222.

26. Tang, J. X. & Janmey, P. A. (1996) Polyelectrolyte nature of F-actin and mechanism of actin bundle formation, *J. Biol. Chem. 271*, 8556−8563.

27. Tang, J. X., Szymanski, P., Janmey, P. A. & Tao, T. (1997) Electrostatic effects of smooth muscle calponin on actin assembly, *Eur. J. Biochem. 247*, 432−440.

28. Tang, J. X., Ito, T., Tao, T., Traub, P. & Janmey, P. A. (1997) Opposite effects of electrostatics and steric exclusion on bundle formation by F-actin and other filamentous polyelectrolytes, *Biochemistry 36*, 12600−12607.

29. Jockusch, B. M. & Isenberg, G. (1981) Interaction of α-actinin and vinculin with actin: opposite effects on filament network formation, *Proc. Natl Acad. Sci. USA 78*, 3005−3009.

30. Ruhnau, K. & Wegner, A. (1988) Evidence for direct binding of vinculin to actin filaments, *FEBS Lett. 228*, 105−108.

31. Westmeyer, A., Ruhnau, K., Wegner, A. & Jockusch, B. M. (1990) Antibody mapping of functional domains in vinculin, *EMBO J. 9*, 2071−2078.

32. Goldmann, W. H., Niggli, V., Kaufmann, S. & Isenberg, G. (1992) Probing actin and liposome interaction of talin and talin-vinculin complexes: A kinetic, thermodynamic and lipid labeling study, *Biochemistry 31*, 7665−7671.

33. Gilmore, A. P. & Burridge, K. (1996) Regulation of vinculin binding to talin and actin by phosphatidylinositol-4,5-bisphosphate, *Nature 381*, 531−535.

34. Schwienbacher, C., Jockusch, B. M. & Ruediger, M. (1996) Intramolecular interactions regulate serine/threonine phosphorylation of vinculin, *FEBS Lett. 384*, 71−74.

35. Weekes, J., Barry, S. T. & Critchley, D. R. (1996) Acidic phospholipids inhibit the intramolecular association between the N- and C-terminal regions of vinculin, exposing actin-binding and protein kinase C phosphorylation sites, *Biochem. J. 314*, 827−832.

36. Craig, S. W. & Johnson, R. P. (1996) Assembly of focal adhesions: progress, paradigms, and portents, *Curr. Opin. Cell Biol. 8*, 74−85.

37. Gilmore, A. P. & Burridge, K. (1996) Molecular mechanisms for focal adhesion assembly through regulation of protein-protein interactions, *Structure 4*, 647−651.

38. Goldmann, W. H., Ezzell, R. M., Adamson E. D., Niggli, V. & Isenberg, G. (1996) Vinculin, talin and focal adhesions, *J. Muscle Res. Cell Motil. 17*, 1−5.

39. Isenberg, G. (1996) New concepts for signal perception and transduction by the actin cytoskeleton at cell boundaries, *Semin. Cell Dev. Biol. 7*, 707−715.

40. Jockusch, B. M. & Ruediger, M. (1996) Crosstalk between cell adhesion: vinculin as a paradigm for regulation by conformation, *Trends Cell Biol. 6*, 311−315.